SGNet: Structure-Aware Graph-Based Network for Airway Semantic Segmentation

Zimeng Tan[1,2], Jianjiang Feng[1,2(✉)], and Jie Zhou[1,2]

[1] Department of Automation, Tsinghua University, Beijing, China
jfeng@tsinghua.edu.cn
[2] Beijing National Research Center for Information Science and Technology, Beijing, China

Abstract. Airway semantic segmentation, which refers to segmenting airway from background and dividing it into anatomical segments, provides clinically valuable information for lung lobe analysis, pulmonary lesion localization, and comparison between different patients. It is technically challenging due to the complicated tree-like structure, individual variations, and severe class imbalance. We propose a structure-aware graph-based network (SGNet) for airway semantic segmentation directly from chest CT scans. The proposed framework consists of a feature extractor combining a multi-task U-Net with a structure-aware GCN, and an inference module comprised of two convolutional layers. The multi-task U-Net is trained to regress bifurcation landmark heatmaps, binary and semantic segmentation maps simultaneously, providing initial predictions for graph construction. By introducing irregular edges connecting voxels with the sampled points around corresponding bifurcation landmarks, the two-layer GCN incorporates the structural prior explicitly. Experiments on both public and private datasets demonstrate that the SGNet achieves superior and robust performance, even on subjects affected by severe pulmonary diseases.

Keywords: Airway semantic segmentation · Graph convolutional network · Structural prior

1 Introduction

Airway segmentation on chest CT scans is crucial for pulmonary disease diagnosis and surgical navigation [5–7]. Airway semantic segmentation (see Fig. 1(b)), which can be regarded as an extension of airway binary segmentation (see Fig. 1(a)), refers to segmenting airway from background and dividing it into 32 anatomical segments defined in [1,2] according to the anatomical topology.

This work was supported in part by the National Natural Science Foundation of China under Grants 82071921.

M. de Bruijne et al. (Eds.): MICCAI 2021, LNCS 12901, pp. 153–163, 2021.
https://doi.org/10.1007/978-3-030-87193-2_15

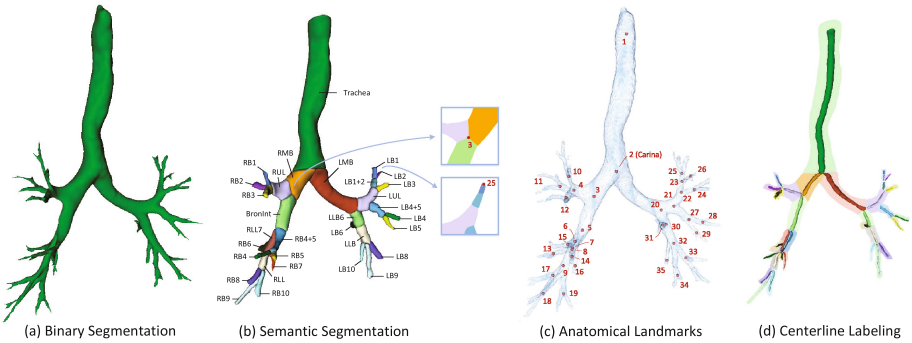

Fig. 1. Illustration of airway binary segmentation, 32 semantic segments, 35 anatomical bifurcation landmarks and centerline labeling.

Airway semantic segmentation can not only capture the whole tree-like structure, but also provide more clinically valuable information for many subsequent automated procedures, such as lung lobe analysis, pulmonary lesion localization, and comparison of the same bronchi from different subjects.

Considering that manual annotation is time-consuming and laborious, several methods based on convolutional neural networks (CNNs) [3,4] have been developed for airway binary segmentation [5–12]. Despite the remarkable progress in binary segmentation, airway semantic segmentation can be much more challenging. Firstly, severe class imbalance occurs naturally due to the sparse distribution of tertiary bronchi, which are very tenuous and tend to be misdetected or undetected. Secondly, there is no obvious interface between adjacent segments (e.g., RMB and RUL in Fig. 1(b)), that is, the voxels around the interface may have similar local appearance and grayscale distribution but different labels. Furthermore, the individual variations, pathological changes, and the large amount of segments contained in an airway tree pose threat to the network training. Another more relevant task is the centerline labeling (see Fig. 1(d)), which takes the extracted centerline as a prerequisite and divides it into different categories for airway [13,14], coronary arteries [15–17], brain arteries [18] and abdominal arteries [19]. An intuitive approach for airway semantic segmentation is to combine binary segmentation with centerline extraction and labeling [13]. Nevertheless, it is not trivial to accomplish these tasks robustly. Completing them independently and integrating results may not achieve the best performance.

Recently, graph convolutional network (GCN) [20] is developed to reason the relationships among sampled points and has already been used in tree-like anatomical structure segmentation [21–25]. Shin et al. [23] combined GCN with a CNN framework to explore global connectivity for 2D vessel segmentation in retinal and coronary artery X-ray images. Juarez et al. [24] replaced the deepest convolutional layer in the U-Net by a series graph convolutions to improve airway binary segmentation. In a more relevant paper, Yao et al. [25] proposed a GCN-based point cloud approach to conduct semantic segmentation of head and neck vessels in CTA images, in which CNN-based binary segmentation is converted

to point cloud and a GCN is employed to further label vessels into 13 major segments. However, only the neighbors on regular image grid are taken into consideration in [25] and the tree-like structural prior has not been fully utilized.

In this paper, we propose an end-to-end deep learning framework, called Structure-aware Graph-based Network (SGNet), for airway semantic segmentation directly from chest CT scans. Specifically, as shown in Fig. 2, a multi-task U-Net is combined with a specially designed GCN for feature extraction and two stacked convolution layers serve as interference module. A total of 35 bifurcation landmarks are predefined at the center of interface between adjacent segments (see Fig. 1(c)) for both auxiliary task of multi-task U-Net and sampling strategy of graph vertices. Our main contributions are summarized as follows: (1) The U-Net is modified to accomplish anatomical landmark detection, airway binary and semantic segmentation simultaneously. The synergy among different objectives guides the network to learn more discriminative features. (2) Based on the initial prediction of the U-Net, graph vertices are sampled randomly on the segments and around the detected landmark positions. Besides the regular edges between vertex and its nearest neighbors, we explore another type of edge connecting each vertex with the points sampled around the corresponding landmarks. In this way, we introduce the structural prior knowledge which boosts the final performance. The voxels' coordinates and distances relative to the carina (shown in Fig. 1(c)) are also fed into the GCN to enrich feature representation. (3) To our knowledge, this is the first paper concentrated on airway semantic segmentation. In order to train and evaluate the proposed system, we have made annotations of 100 CT scans, in which the annotations of 60 public CT scans are released to promote further study of airway semantic segmentation[1]. Experiments on both public and private datasets demonstrated that our proposed method achieves superior performance on airway semantic segmentation, even on subjects affected by severe pulmonary diseases such as COVID-19 and interstitial pneumonia.

2 Method

2.1 Multi-task U-Net Module

Given an input 3D volume, we exploit a modified multi-task U-Net [3] to obtain the coarse initial prediction of airway semantic segmentation. Based on the generic pipeline of pixel-wise classification approach, we introduce landmark detection and airway binary segmentation as auxiliary objectives to guide the network to learn more discriminative features. A total of 35 anatomical landmarks are predefined at the interface center of adjacent semantic classes, so that each segment can be expressed by the two points at its ends. Inspired by [26], we convert landmark detection object to a heatmap regression task. Compared with regressing coordinates directly, the voxel-to-voxel heatmap regression

[1] Annotations are available at https://cloud.tsinghua.edu.cn/d/43bbc05fb9714f71a56f/

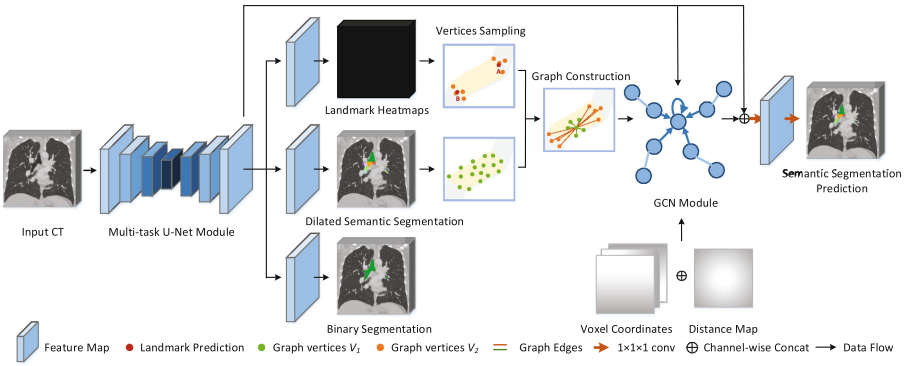

Fig. 2. Overview of the proposed SGNet for airway semantic segmentation.

method focuses on each position and is more suitable intrinsically for landmark localization. The discrete coordinates of each landmark are modeled to a channel heatmap with a Gaussian distribution centered at the position. The heatmap value $G_k(x)$ of voxel x ranging in $[0, 1]$ can be regarded as the probability to be the kth landmark, which is determined according to the standard deviation δ and the distance from the position x to the target landmark x_k. During inference, the voxel with maximum predicted probability is chosen to be the corresponding landmark position. Specifically, the formulation of the heatmap is as follows:

$$G_k(x) = e^{-\frac{1}{2\delta^2}(x-x_k)^2}, k = 1, 2, ..., 35. \tag{1}$$

For airway binary segmentation, it should be noted that unlike the original binary segmentation task, only the 32 predefined anatomical segments are taken into consideration and the peripheral bronchioles are omitted. In this way, the auxiliary objectives are highly correlated with the main task, and the synergy among them boosts the individual performance of each task. Furthermore, we introduce the global context information by capturing the whole airway structure and incorporate the spatial relationships among landmarks implicitly.

2.2 Structure-Aware Graph Convolutional Network

Graph Construction. Based on the initial prediction of airway semantic segmentation S_1 and landmark detection L_1 obtained from the multi-task U-Net, we construct a structure-aware graph $G(V, E)$, where $V = \{v_i\}_{i=1}^{N}$ and E are sets of vertices and edges, respectively. As shown in Fig. 2, we have two types of vertices, one is sampled randomly from the whole segmented airway region and denoted by $V_1 = \{v_i\}_{i=1}^{N_1}$, the other is sampled around the detected landmark positions and denoted by $V_2 = \{v_i\}_{i=1}^{N_2}$, where $N_1 + N_2 = N$. The sampling density of vertices V_1 varies with different segments to pay extra attention to the tenuous tertiary bronchi. Each vertex $v_i \in V$ is linked with its k-nearest

neighbors in the Euclidean space. Besides this regular connectivity, we propose an additional edge between per vertex $v_i \in V_1$ and point $v_j \in V_2$ sampled around the corresponding detected landmarks according to its predicted semantic class $S_1(v_i)$. Specifically, if vertex v_i is classified on the lth segment (i.e. $S_1(v_i) = l$), it should be connected with the vertices sampled around the two endpoints x_A and x_B (see Fig. 2). These novel edges introduce the airway structural prior information explicitly, allowing vertices to access faraway but meaningful neighbors. Moreover, connecting with a series points distributed around the landmark prediction brings a degree of error tolerance in landmark detection.

Graph Convolutional Network. A two-layer graph convolutional network (GCN) [20] operating on the constructed graph $G(V, E)$ is adopted for further feature extraction in our framework. Input feature vector of each vertex is sampled from the immediate feature map $F_0 \in \mathbb{R}^{h \times w \times d \times C_1}$, which is generated by the convolutional layer in the multi-task U-Net before the three branch subnetworks. To enrich feature representation, the voxels' coordinates in 3 dimensions and distances relative to the carina prediction, which is always detected accurately in experiments, are also fed into the input. The matrix of all input feature vectors is denoted as $F_1 \in \mathbb{R}^{N \times (C_1+4)}$. The binary adjacency matrix $A \in \{1, 0\}^{N \times N}$ can be obtained from the constructed graph, which is largely sparse with non-zero entries corresponding to the predefined edges. Then the degree matrix D is derived from A with diagonal entries $D_{ii} = \sum_j A_{ij}$. The two-layer graph convolutional network with self connections is formulated as:

$$F_2 = \sigma\left(\hat{A}\,\sigma\left(\hat{A}F_1W^{(0)}\right)W^{(1)}\right) \tag{2}$$

where $\tilde{A} = A + I_N, \tilde{D}_{ii} = \sum_j \tilde{A}_{ij}$, and $\hat{A} = \tilde{D}^{-\frac{1}{2}}\tilde{A}\tilde{D}^{-\frac{1}{2}}$. $\sigma(\cdot)$ is the rectified linear unit activation function. $W^{(0)}$ and $W^{(1)}$ are trainable filter weights. F_2 is the output feature representation.

Unlike standard convolution operating on a local regular grid, graph convolution intuitively enables irregular information exchange on extracted graph and hence guarantees a much wider receptive field. Benefiting from the specially designed graph, the GCN module can capture more discriminative structural features. To conduct final inference for airway semantic segmentation, we convert the output feature matrix $F_2 \in \mathbb{R}^{N \times C_2}$ to a sparse matrix form $F3 \in \mathbb{R}^{h \times w \times d \times C_2}$ by projecting the feature vector of each vertex to the corresponding voxel position. Then the feature map F_0 from the U-Net and F_3 from the GCN are concatenated channel-wise and fed into the interference module, which consists of two $1 \times 1 \times 1$ convolutional layers followed by non-linear activation function.

2.3 Loss Functions and Training Methodology

We apply weighted L2 loss, cross-entropy loss, and Dice loss function [27] for landmark detection, binary segmentation and semantic segmentation in both the U-Net module and the whole SGNet, respectively. To address the class imbalance issue, the weights are set to be the voxel number ratio of the background class

Table 1. Quantitative results on both public and private test set evaluated using mean Dice coefficient (%) and standard deviation.

Public dataset								
Trachea	RMB	RUL	BronInt	RB1	RB2	RB3	RB4+5	RB4
91.3(5.25)	83.4(4.78)	82.5(4.76)	83.6(4.80)	84.2(4.83)	83.3(4.86)	81.8(4.70)	79.9(4.57)	84.5(5.43)
RB5	RB6	RLL7	RB7	RLL	RB8	RB9	RB10	LMB
81.7(4.73)	74.6(4.35)	80.2(4.60)	85.8(4.83)	80.5(4.62)	74.6(4.35)	88.4(5.11)	86.8(5.01)	82.5(4.90)
LUL	LLB6	LB1+2	LB1	LB2	LB3	LB4+5	LB4	LB5
77.8(4.50)	77.7(4.46)	83.2(4.83)	85.8(5.34)	84.8(5.06)	68.8(3.82)	80.7(4.62)	86.4(5.55)	86.1(5.01)
LB6	LLB	LB8	LB9	LB10	Average		Overall	
78.8(4.57)	81.2(4.66)	70.3(3.95)	83.4(4.72)	78.1(4.57)	81.7(4.76)		89.3(1.96)	
Private dataset								
Trachea	RMB	RUL	BronInt	RB1	RB2	RB3	RB4+5	RB4
90.9(2.63)	82.8(2.37)	82.0(2.36)	82.1(2.31)	76.9(2.16)	78.5(2.25)	78.5(2.27)	79.6(2.28)	76.3(2.21)
RB5	RB6	RLL7	RB7	RLL	RB8	RB9	RB10	LMB
73.9(2.13)	78.0(2.22)	75.8(2.13)	70.5(2.01)	78.8(2.27)	72.8(2.17)	62.6(1.79)	65.9(1.82)	80.2(2.33)
LUL	LLB6	LB1+2	LB1	LB2	LB3	LB4+5	LB4	LB5
76.0(2.21)	75.3(2.15)	68.1(2.15)	73.2(2.24)	7.14(2.18)	67.7(2.03)	71.3(2.13)	85.0(2.42)	80.8(2.35)
LB6	LLB	LB8	LB9	LB10	Average		Overall	
74.9(2.12)	77.7(2.24)	71.3(2.04)	70.4(2.09)	84.2(2.39)	76.0(2.20)		88.5(1.61)	

to each type of foreground. We adopt a sequential training scheme composed of initial pretraining of the U-Net and joint training of the whole framework. The objective functions of the U-Net module and the SGNet are defined as:

$$\mathcal{L}_{U-Net} = \mathcal{L}_{land} + \alpha\mathcal{L}_{bseg} + \beta\mathcal{L}_{sseg-ini} \tag{3}$$

$$\mathcal{L}_{SGNet} = \mathcal{L}_{U-Net} + \gamma\mathcal{L}_{sseg-final} \tag{4}$$

where the hyper-parameters α, β, and γ are adjusted to make different components having the same scale. Similar to [25], we dilate the ground truth mask of semantic segmentation in the U-Net, ensuring inclusion of all meaningful voxels in the GCN sampling stage and improving the performance especially around the airway wall. During training, the vertices set V_2 is sampled around the ground truth landmark positions to avoid unnecessary disturbance. During inference, the landmark predictions of the U-Net are utilized for graph construction.

3 Experiments and Results

3.1 Datasets and Implementation Details

Datasets. We evaluated our approach on both public and private chest CT datasets. The public dataset [6] is comprised of 40 scans from LIDC-IDRI [28] and 20 scans from EXACT'09 [29], with airway binary segmentation annotation provided. The private dataset contains 40 scans with 10 kinds of severe pulmonary diseases (e.g. COVID-19, pulmonary cryptococcosis, interstitial pneumonia and adenocarcinoma). 35 bifurcation anatomical landmarks and binary

Table 2. Comparison of different networks on both public and private test set measured by DSC (%), TPR (%), and FPR (10^{-4}). The U-Net, mU-Net, and +GCN represent the original U-Net, the proposed multi-task U-Net, and the combination of the multi-task U-Net and a GCN with regular connectivity, respectively.

Public dataset															
Models	Trachea			Primary			Lobar			Tertiary			Average		
	DSC	TPR	FPR	DSC	TPR	FPR	DSC	TPR	FPR	DSC	TPR	FPR	DSC	TPR	FPR
U-Net	88.7	84.1	1.66	79.2	73.0	**0.51**	74.9	71.1	0.20	73.6	73.7	0.07	74.7	73.3	0.18
mU-Net	89.3	85.1	1.66	80.5	74.6	0.55	77.6	76.1	0.24	76.3	77.6	0.07	77.3	77.3	0.19
+GCN	90.5	86.6	1.5	81.5	80.2	0.69	78.7	75.6	0.19	79.9	79.6	0.05	80.0	78.8	0.17
SGNet	**91.3**	**88.0**	**1.48**	**83.0**	**81.5**	0.67	**80.4**	**77.6**	**0.18**	**81.6**	**79.7**	**0.04**	**81.7**	**79.5**	**0.16**
Private dataset															
Models	Trachea			Primary			Lobar			Tertiary			Average		
	DSC	TPR	FPR	DSC	TPR	FPR	DSC	TPR	FPR	DSC	TPR	FPR	DSC	TPR	FPR
U-Net	90.2	88.0	3.37	77.5	70.3	0.56	75.4	73.9	0.30	63.1	70.2	0.11	67.9	71.6	0.28
mU-Net	90.3	88.4	3.29	77.3	70.1	**0.53**	75.3	74.4	0.27	65.5	70.1	0.07	69.4	71.7	0.25
+GCN	90.7	89.2	2.50	80.2	74.4	0.57	77.8	75.8	0.26	71.6	72.4	**0.06**	74.3	73.9	0.22
SGNet	**90.9**	**89.8**	**2.20**	**81.5**	**76.1**	0.56	**78.4**	**76.3**	**0.24**	**73.9**	**73.7**	0.06	**76.0**	**75.0**	**0.20**

segmentation (only for private dataset) were annotated by well-trained experts. Based on the binary segmentation annotation, the airway semantic segmentation ground truth of each CT scan was established automatically according to the landmark distribution, followed by manual correction and delineation. All scans were spatially normalized to the same resolution of $0.7 \times 0.7 \times 1$ mm^3 with average size of $486 \times 486 \times 317$. The datasets were randomly split into training set (40 public and 30 private scans) and test set (20 public and 10 private scans).

Implementation Details. To improve the model's generalizability, we applied data augmentation via random translation and rotation for 3 times totally on the training set. We trained our U-Net module and SGNet using Adam optimizer ($\beta_1 = 0.5, \beta_2 = 0.999$) with a learning rate of 0.0001 for 100 and 50 epochs, respectively. For hyper-parameters, we empirically set $\alpha = 10^{-3}, \beta = 10^{-7}$, and $\gamma = 10^{-5}$. For the constructed graph, we randomly sampled 1024 points for each airway tree to form vertex set V_1 and 8 points around each bifurcation landmark to form vertex set V_2. Each vertex is connected with its 16-nearest neighbors in V_1 and the vertices located around the corresponding two endpoints in V_2. The proposed model was implemented in TensorFlow framework with 2 NVIDIA GeForce RTX 3090 GPUs.

3.2 Results

The performance of the proposed SGNet was evaluated utilizing Dice coefficient, and the quantitative results on both public and private test sets are presented in Table 1. The overall Dice coefficient refers to converting the semantic segmentation prediction to binary form by regarding voxels classified in airway segments

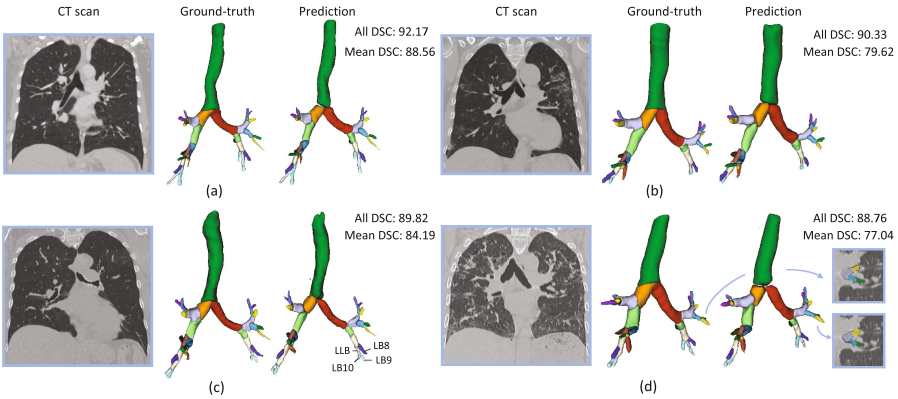

Fig. 3. Qualitative results of (a) a public test case, (b) a private test case, (c) individual variations of airway anatomical topology, and (d) pathological effects of severe pulmonary diseases.

as foreground, and then comparing with the ground truth. The average Dice coefficient indicates the mean of all airway segments. The qualitative results of 4 patients are illustrated in Fig. 3. The proposed SGNet achieves satisfactory performance on most airway segments (see Fig. 3(a) and (b)), while some failure cases may be ascribed to the sparse distribution of complicated airway structure, tenuous tertiary bronchi, and individual variations of airway anatomical topology (e.g. in some subjects, as shown in Fig. 3(a), LB8-LB10 diverge from LLB simultaneously, while in others, as shown in Fig. 3(c), LB8 first diverges from LLB, and then LLB is divided into LB9 and LB10. A similar situation can be seen in RB8-RB10.). There are some ruptures between the adjacent airway segments, which may be improved by taking voxel-wise spatial connectivity into account and will be explored in future work. Meanwhile, the performance on the private dataset shows a slight decrease. It is intuitively more difficult due to the pathological effects of severe pulmonary diseases, such as the indistinct airway wall and changes of the lung grayscale distribution (e.g. see Fig. 3(d) from a patient with interstitial pneumonia). The experimental results demonstrate the effectiveness and robustness of the proposed framework on challenging cases.

Furthermore, we conducted an ablation study to verify each component of our proposed framework. For a more comprehensive comparison, we additionally introduced true positive rate (TPR) and false positive rate (FPR) together with Dice coefficient (DSC) as evaluation metrics. For demonstration purpose, we divided 32 airway anatomical segments into 4 groups and computed the average metrics of each one, i.e., trachea, primary bronchi (including LMB and RMB), lobar bronchi (including BronInt, RUL, RB4+5, RLL7, RLL, LUL, LLB6, LLB), and tertiary bronchi (including RB1-RB10, LB1+2, LB4+5, LB1-LB6, LB8-LB10). Note that in order to cover all the segments, there are slight differences between this division and anatomical definition (e.g. we classified BronInt to the lobar bronchi group). We compared the performance of four different

networks: the original U-Net trained for airway semantic segmentation, the proposed multi-task U-Net, combination of the multi-task U-Net and a GCN with regular connectivity, and the proposed SGNet. Results on both public and private test sets are presented in Table 2, where the last 4 columns represent the average measurements on all 32 segments. The proposed SGNet achieved the highest DSC and TPR of each airway segment on both test sets with comparable FPR. Adding auxiliary objectives, combining with GCN, and introducing the structure-aware connectivity successively improves the average DSC by 2.6%, 2.7%, 1.7%, and 1.5%, 4.9%, 1.7% on public and private datasets, respectively. It implies that integrating global context information and introducing structural prior knowledge explicitly contribute to the overall performance improvement, demonstrating the effectiveness of the proposed framework.

4 Conclusion

In this paper, we presented an end-to-end structure-aware graph-based network (SGNet) for airway semantic segmentation directly from chest CT scans, in which a multi-task U-Net and a GCN are combined for more discriminative feature extraction. The structural prior knowledge was incorporated explicitly by introducing irregular graph connectivity. Experiments showed the effectiveness and robustness of the proposed method on both public and private datasets. In the future, we will extend our framework to other tree-like anatomical structures and perform a more comprehensive comparison with related techniques.

References

1. van Ginneken, B., Baggerman, W., van Rikxoort, E.M.: Robust segmentation and anatomical labeling of the airway tree from thoracic CT scans. In: Metaxas, D., Axel, L., Fichtinger, G., Székely, G. (eds.) MICCAI 2008. LNCS, vol. 5241, pp. 219–226. Springer, Heidelberg (2008). https://doi.org/10.1007/978-3-540-85988-8_27
2. Tschirren, J., McLennan, G., Palágyi, K., et al.: Matching and anatomical labeling of human airway tree. IEEE T-MI **24**(12), 1540–1547 (2005)
3. Ronneberger, O., Fischer, P., Brox, T.: U-Net: convolutional networks for biomedical image segmentation. In: Navab, N., Hornegger, J., Wells, W.M., Frangi, A.F. (eds.) MICCAI 2015. LNCS, vol. 9351, pp. 234–241. Springer, Cham (2015). https://doi.org/10.1007/978-3-319-24574-4_28
4. Çiçek, Ö., Abdulkadir, A., Lienkamp, S.S., Brox, T., Ronneberger, O.: 3D U-Net: learning dense volumetric segmentation from sparse annotation. In: Ourselin, S., Joskowicz, L., Sabuncu, M.R., Unal, G., Wells, W. (eds.) MICCAI 2016. LNCS, vol. 9901, pp. 424–432. Springer, Cham (2016). https://doi.org/10.1007/978-3-319-46723-8_49
5. Qin, Y., et al.: AirwayNet: a voxel-connectivity aware approach for accurate airway segmentation using convolutional neural networks. In: Shen, D., et al. (eds.) MICCAI 2019. LNCS, vol. 11769, pp. 212–220. Springer, Cham (2019). https://doi.org/10.1007/978-3-030-32226-7_24

6. Qin, Y., Gu, Y., Zheng, H., et al.: AirwayNet-SE: a simple-yet-effective approach to improve airway segmentation using context scale fusion. In: ISBI (2020)
7. Qin, Y., et al.: Learning bronchiole-sensitive airway segmentation CNNs by feature recalibration and attention distillation. In: Martel, A.L., et al. (eds.) MICCAI 2020. LNCS, vol. 12261, pp. 221–231. Springer, Cham (2020). https://doi.org/10.1007/978-3-030-59710-8_22
8. Charbonnier, J.P., Van Rikxoort, E.M., Setio, A.A., et al.: Improving airway segmentation in computed tomography using leak detection with convolutional networks. MedIA **36**, 52–60 (2017)
9. Meng, Q., Roth, H.R., Kitasaka, T., Oda, M., Ueno, J., Mori, K.: Tracking and segmentation of the airways in chest CT using a fully convolutional network. In: Descoteaux, M., Maier-Hein, L., Franz, A., Jannin, P., Collins, D.L., Duchesne, S. (eds.) MICCAI 2017. LNCS, vol. 10434, pp. 198–207. Springer, Cham (2017). https://doi.org/10.1007/978-3-319-66185-8_23
10. Yun, J., Park, J., Yu, D., et al.: Improvement of fully automated airway segmentation on volumetric computed tomographic images using a 2.5 dimensional convolutional neural net. MedIA **51**, 13–20 (2019)
11. Wang, C., et al.: Tubular structure segmentation using spatial fully connected network with radial distance loss for 3D medical images. In: Shen, D., et al. (eds.) MICCAI 2019. LNCS, vol. 11769, pp. 348–356. Springer, Cham (2019). https://doi.org/10.1007/978-3-030-32226-7_39
12. Zhao, T., Yin, Z., Wang, J., Gao, D., Chen, Y., Mao, Y.: Bronchus segmentation and classification by neural networks and linear programming. In: Shen, D., et al. (eds.) MICCAI 2019. LNCS, vol. 11769, pp. 230–239. Springer, Cham (2019). https://doi.org/10.1007/978-3-030-32226-7_26
13. Gu, S., Wang, Z., Siegfried, J.M., et al.: Automated lobe-based airway labeling. Int. J. Biomed. Imaging **2012** (2012)
14. Feragen, A.: A hierarchical scheme for geodesic anatomical labeling of airway trees. In: Ayache, N., Delingette, H., Golland, P., Mori, K. (eds.) MICCAI 2012. LNCS, vol. 7512, pp. 147–155. Springer, Heidelberg (2012). https://doi.org/10.1007/978-3-642-33454-2_19
15. Wu, D., et al.: Automated anatomical labeling of coronary arteries via bidirectional tree LSTMs. Int. J. Comput. Assist. Radiol. Surg. **14**(2), 271–280 (2018). https://doi.org/10.1007/s11548-018-1884-6
16. Yang, H., Zhen, X., Chi, Y., et al.: CPR-GCN: conditional partial-residual graph convolutional network in automated anatomical labeling of coronary arteries. In: CVPR (2020)
17. Cao, Q., et al.: Automatic identification of coronary tree anatomy in coronary computed tomography angiography. Int. J. Cardiovasc. Imaging **33**(11), 1809–1819 (2017). https://doi.org/10.1007/s10554-017-1169-0
18. Robben, D., Türetken, E., Sunaert, S., et al.: Simultaneous segmentation and anatomical labeling of the cerebral vasculature. MedIA **32**, 201–215 (2016)
19. Matsuzaki, T., Oda, M., Kitasaka, T., et al.: Automated anatomical labeling of abdominal arteries and hepatic portal system extracted from abdominal CT volumes. MedIA **20**(1), 152–161 (2015)
20. Kipf, T.N., Welling, M.: Semi-supervised classification with graph convolutional networks. In: ICLR (2017)
21. Selvan, R., Kipf, T., Welling, M., et al.: Extraction of airways using graph neural networks. In: MIDL (2018)
22. Selvan, R., Kipf, T., Welling, M., et al.: Graph refinement based airway extraction using mean-field networks and graph neural networks. MedIA **64**, 101751 (2020)

23. Shin, S.Y., Lee, S., Yun, I.D., et al.: Deep vessel segmentation by learning graphical connectivity. MedIA **58**, 101556 (2019)
24. Juarez, A.G.U., Selvan, R., Saghir, Z., de Bruijne, M.: A joint 3D unet-graph neural network-based method for airway segmentation from chest CTs. In: MLMI (2019)
25. Yao, L., Jiang, P., Xue, Z., et al.: Graph convolutional network based point cloud for head and neck vessel labeling. In: MLMI (2020)
26. Payer, C., Štern, D., Bischof, H., Urschler, M.: Regressing heatmaps for multiple landmark localization using CNNs. In: Ourselin, S., Joskowicz, L., Sabuncu, M.R., Unal, G., Wells, W. (eds.) MICCAI 2016. LNCS, vol. 9901, pp. 230–238. Springer, Cham (2016). https://doi.org/10.1007/978-3-319-46723-8_27
27. Milletari, F., Navab, N., Ahmadi, S.A.: V-net: fully convolutional neural networks for volumetric medical image segmentation. In: 3DV (2016)
28. Armato, I.I.I., Samuel, G., et al.: The lung image database consortium (LIDC) and image database resource initiative (IDRI): a completed reference database of lung nodules on CT scans. Med. Phys. **38**(2), 915–931 (2011)
29. Lo, P., Ginneken, B.V., Reinhardt, J.M., et al.: Extraction of airways from CT (EXACT'09). IEEE T-MI **31**(11), 2093–2107 (2012)